

# Direct collapse to supermassive black hole seeds: the critical conditions for suppression of H<sub>2</sub> cooling

Yang Luo,<sup>1★</sup> Isaac Shlosman,<sup>2,3</sup> Kentaro Nagamine<sup>3,4,5</sup> and Taotao Fang<sup>1</sup>

<sup>1</sup>*Department of Astronomy and Institute of Theoretical Physics and Astrophysics, Xiamen University, Xiamen, Fujian 361005, China*

<sup>2</sup>*Department of Physics & Astronomy, University of Kentucky, Lexington, KY 40506-0055, USA*

<sup>3</sup>*Theoretical Astrophysics, Department of Earth & Space Science, Osaka University, 1-1 Machikaneyama, Toyonaka, Osaka 560-0043, Japan*

<sup>4</sup>*Department of Physics & Astronomy, University of Nevada, Las Vegas, NV 89154-4002, USA*

<sup>5</sup>*Kavli-IPMU (WPI), University of Tokyo, 5-1-5 Kashiwanoha, Kashiwa, Chiba, 277-8583, Japan*

Accepted XXX. Received YYY; in original form ZZZ

## ABSTRACT

Observations of high-redshift quasars imply the presence of supermassive black holes (SMBHs) already at  $z \sim 7.5$ . An appealing and promising pathway to their formation is the direct collapse scenario of a primordial gas in atomic-cooling haloes at  $z \sim 10-20$ , when the H<sub>2</sub> formation is inhibited by a strong background radiation field, whose intensity exceeds a critical value,  $J_{\text{crit}}$ . To estimate  $J_{\text{crit}}$ , idealized spectra have been assumed, with a fixed ratio of H<sub>2</sub> photo-dissociation rate  $k_{\text{H}_2}$  to the H<sup>−</sup> photo-detachment rate  $k_{\text{H}^-}$ . This assumption, however, could be too narrow in scope as the nature of the background radiation field is not known precisely. In this work we show that the critical condition for suppressing the H<sub>2</sub> cooling in the collapsing gas could be described in a more general way by a combination of  $k_{\text{H}_2}$  and  $k_{\text{H}^-}$  parameters, without any additional assumptions about the shape of the underlying radiation spectrum. By performing a series of cosmological zoom-in simulations with an encompassing set of  $k_{\text{H}_2}$  and  $k_{\text{H}^-}$ , we examine the gas flow by following evolution of basic parameters of the accretion flow. We test under what conditions the gas evolution is dominated by H<sub>2</sub> and/or atomic cooling. We confirm the existence of a critical curve in the  $k_{\text{H}_2} - k_{\text{H}^-}$  plane, and provide an analytical fit to it. This curve depends on the conditions in the direct collapse, and reveals domains where the atomic cooling dominates over the molecular cooling. Furthermore, we have considered the effect of H<sub>2</sub> self-shielding on the critical curve, by adopting three methods for the effective column density approximation in H<sub>2</sub>. We find that the estimate of the characteristic length-scale for shielding can be improved by using  $\lambda_{\text{Jeans}25}$ , which is 0.25 times that of the local Jeans length.

**Key words:** methods: numerical — galaxies: formation — galaxies: high-redshift — cosmology: theory — cosmology: dark ages, reionization, first stars — quasars: supermassive black holes

## 1 INTRODUCTION

Supermassive black holes (SMBHs) with masses of  $\sim 10^9 M_{\odot}$  have been found in the less than 750 Myr-old universe, at  $z \sim 7.5$ , in the midst of quasars (Fan et al. 2003; Mortlock et al. 2011; Willott et al. 2010; Wu et al. 2015; Venemans et al. 2017; Bañados et al. 2018). The origin of these SMBHs is still an open question, and it is not clear how they have managed to grow so quickly after the Big Bang.

The SMBH seeds can in principle grow via supercritical

accretion from stellar mass black holes — the end products of metal-free Population III stars. But this growth rate requires a massive reservoir of accretion matter feeding the Pop III remnant over long time intervals, e.g., longer than 100 Myr. Such an option can be realized in the form of a supermassive star (Volonteri & Rees 2006; Begelman et al. 2006; Begelman 2010), but its existence must be verified in the first place. Another possibility is the runaway collapse of compact stellar clusters, subject to general relativistic effects (Zel'dovich & Podurets 1965; Shapiro & Teukolsky 1985), or stellar/gas dynamical evolution of stellar clusters (Begelman & Rees 1978; Lupi et al. 2014). Their existence

★ E-mail: yangluo@xmu.edu.cn (YL)

at high redshifts requires explanation and their evolution is a subject to a fine tuning.

The most realistic method to form the SMBH seeds at present remains the direct collapse scenario, which involves the baryonic collapse within dark matter (DM) haloes to form the SMBH seeds of  $\sim 10^4 - 10^6 M_\odot$  (Rees 1984; Haehnelt & Rees 1993; Loeb & Rasio 1994; Bromm & Loeb 2003; Koushiappas et al. 2004; Begelman et al. 2006; Volonteri & Rees 2006; Begelman et al. 2008; Begelman & Shlosman 2009; Begelman 2010; Milosavljević et al. 2009; Mayer et al. 2010; Johnson et al. 2011; Choi et al. 2013, 2015; Latif et al. 2013, 2014b; Chon et al. 2016; Luo et al. 2016, 2018; Shlosman et al. 2016; Ardanesh et al. 2018).

In the direct collapse scenario, the virial temperature of DM haloes must exceed the cooling floor of the primordial gas. The collapsing flow must also be prevented from forming the molecular hydrogen. Otherwise, the  $H_2$  cooling can lead to fragmentation and formation of Pop III stars, thus preventing formation of a massive central black hole seed (Haiman et al. 2000; Wise & Abel 2008; Begelman & Shlosman 2009; Regan & Haehnelt 2009; Greif et al. 2011; Latif et al. 2016; Regan & Downes 2018). Numerical simulations of an optically-thin collapse have confirmed that in the absence of a molecular cooling, the gas stays isothermal, at the atomic hydrogen cooling floor (Omukai 2001; Bromm & Loeb 2003; Shang et al. 2010; Choi et al. 2013, 2015; Latif et al. 2013; Choi et al. 2013; Latif et al. 2016; Shlosman et al. 2016).

Suppression of the  $H_2$  cooling requires the presence of a strong UV background radiation field, which can dissociate  $H_2$  and prevent its formation. In most studies, the minimum value of the UV intensity to suppress the  $H_2$  cooling is denoted by  $J_{\text{crit}}$ , in units of  $J_{\text{LW},21} = 10^{-21} \text{ erg s}^{-1} \text{ cm}^{-2} \text{ Hz}^{-1} \text{ sr}^{-1}$ . The UV background intensity in the early universe is expected to come from the cosmic star formation (e.g., Greif et al. 2007; Haardt & Madau 2012). Subsequent analysis has indicated that the background intensity may not be strong enough to reach the required  $J_{\text{crit}}$  (e.g. Ciardi et al. 2000; Ciardi & Ferrara 2005; Dijkstra et al. 2008; Ahn et al. 2009; Holzbauer & Furlanetto 2012).

To assure that the collapsing gas within a DM halo will be able to follow the isothermal track, the direct collapse haloes must be located close to the starforming galaxies (e.g., Agarwal et al. 2012; Dijkstra et al. 2014), in order to be subject to a strong UV flux. However, attempts to search for such haloes and obtain their population have encountered extreme difficulties (e.g., Yue et al. 2013; Chon & Latif 2017; Habouzit et al. 2016). The estimate of the number density of direct collapse haloes at  $z \sim 10$  exposed to radiation from a nearby starforming galaxy is very sensitive to  $J_{\text{crit}}$  (e.g., Dijkstra et al. 2008; Agarwal et al. 2012; Dijkstra et al. 2014; Yue et al. 2014; Inayoshi & Tanaka 2015; Yue et al. 2017). A variation by an order of magnitude in  $J_{\text{crit}}$  can lead to the five orders of magnitude variation in this probability. This emphasizes the need to obtain a more stringent constraint on the value of  $J_{\text{crit}}$  and on the uncertainties in its determination.

The value of  $J_{\text{crit}}$  is strongly dependent on the background radiation spectral shape. Hence, it depends on the relative contribution from  $H^-$  photo-detachment

rate,  $k_{H^-}$ , and from  $H_2$  photo-dissociation rate,  $k_{H_2}$  (e.g., Sugimura et al. 2014). For a given radiation spectral shape,  $k_{H^-}$  and  $k_{H_2}$  can be calculated from

$$k_{H^-} = \alpha \kappa_{H^-} J_{\text{LW}} \quad (1)$$

$$k_{H_2} = \beta \kappa_{H_2} J_{\text{LW}}, \quad (2)$$

where  $\kappa_{H^-} \approx 1.1 \times 10^{-10} \text{ s}^{-1}$  and  $\kappa_{H_2} \approx 1.38 \times 10^{-12} \text{ s}^{-1}$  are the rate coefficients of  $H^-$  photo-detachment and  $H_2$  photo-dissociation, respectively (e.g., Abel et al. 1997; Glover & Jappsen 2007; Miyake et al. 2010). Dimensionless parameters  $\alpha$  and  $\beta$  provide the dependence on the radiation spectral shape (Glover & Jappsen 2007). When the specific intensity at 13.6 eV becomes larger than  $J_{\text{crit}}$ , the  $H_2$  cooling can be inhibited.

In most cases, the estimate of  $J_{\text{crit}}$  is obtained by assuming a particular spectral shape, either a blackbody or a power law. For Pop III star galaxies, the radiation field has been modeled as a blackbody with  $T_\star = 10^5 \text{ K}$ , hereafter referred to as T5 (Omukai 2001; Shang et al. 2010; Hartwig et al. 2015a; Inayoshi & Tanaka 2015). For a Pop II starforming galaxy, the blackbody has been assumed to have  $T_\star = 10^4 \text{ K}$ , hereafter referred to as T4 (Omukai 2001; Shang et al. 2010; Latif et al. 2014a; Inayoshi & Tanaka 2015). The values of  $J_{\text{crit}}$ , in units of  $J_{\text{LW},21}$ , obtained in previous studies span a large range, from as low as 20 to as high as  $10^5$ , depending on the incident radiation spectral shape, and the treatment of the  $H_2$  self-shielding (Shang et al. 2010; Wolcott-Green et al. 2011; Sugimura et al. 2014; Latif et al. 2014a; Hartwig et al. 2015a; Inayoshi & Tanaka 2015; Glover 2015b; Regan et al. 2016; Agarwal et al. 2016; Wolcott-Green et al. 2017; Dunn et al. 2018).

For the T5 and T4 blackbody spectra, the ratio of  $k_{H^-}$  to  $k_{H_2}$  is fixed. However, in realistic situations, the background radiation spectrum is expected to evolve, and hence both  $k_{H^-}$  and  $k_{H_2}$  will be changing with time. Moreover, trapping of  $\text{Ly}\alpha$  photons emitted in an optically-thick accretion flow during the direct collapse can affect the gas cooling (e.g., Schleicher et al. 2010; Ge & Wise 2017), and even photo-detach most of  $H^-$  (e.g., Johnson & Dijkstra 2017). Under these conditions, the ratio of  $k_{H^-}$  to  $k_{H_2}$  cannot be calculated simply.

Additionally, the value of  $J_{\text{crit}}$  depends on the treatment of  $H_2$  self-shielding (Wolcott-Green et al. 2011; Hartwig et al. 2015a). With an increasing  $H_2$  number density, the molecular gas can self-shield the background radiation, and reduce the effect of photo-dissociation. Most numerical simulations used the local Jeans length to calculate the column densities for self-shielding, but this assumption can lead to an overestimate of  $J_{\text{crit}}$  (e.g., Wolcott-Green et al. 2011). In three-dimensional (3D) simulations, the self-shielding depends on the direction as well, due to a spatial variation of the gas density and its temperature. This direction dependence can cause a substantial difference in the estimate of  $J_{\text{crit}}$ , between 3D and 1D simulations (e.g., Shang et al. 2010; Latif et al. 2014a). Moreover, existence of the X-rays could increase the hydrogen ionization fraction and the free electron fraction, which promotes the  $H^-$  and  $H_2$  formation via the electron-catalysed reactions. The effect of extragalactic X-ray background could increase the value of  $J_{\text{crit}}$  by a factor of 3 to 10, depending on the spectral shape of the background UV radiation (Inayoshi & Haiman 2014; Latif et al. 2015; Glover 2016).

Other uncertainties, like chemical reactions (Glover 2015a), the rate coefficient of the collisional ionization of hydrogen (Glover 2015b), and anisotropy in the external radiation (Regan et al. 2016) could also introduce an uncertainty of up to a factor of 5 into the determination of  $J_{\text{crit}}$ . Therefore, a more general way to calculate  $J_{\text{crit}}$  is required.

The critical intensity lacks a unique value, and can be determined by a combination of  $k_{\text{H}^-}$  and  $k_{\text{H}_2}$ , on a two-dimensional plane. For a given  $k_{\text{H}^-}$ , a critical value of  $k_{\text{H}_2}$  is expected to exist, above which the H<sub>2</sub> cooling will be suppressed. A critical curve has been found in the  $k_{\text{H}^-}$  and  $k_{\text{H}_2}$  plane for 1D simulations (Agarwal et al. 2016; Wolcott-Green et al. 2017). This curve provides a more general way of determining the critical conditions, without any assumptions of the shape of the underlying radiation spectrum. But a question remains about the existence of such a curve in 3D simulations. How does the critical curve depend on the spatial variations in the density and temperature in 3D? What is the effect of the H<sub>2</sub> self-shielding approximation on the shape of this curve? In this work, we investigate the dependence of  $J_{\text{crit}}$  on the  $k_{\text{H}^-}$  and  $k_{\text{H}_2}$  in the 3D cosmological zoom-in simulations. We also analyze the sensitivity of  $J_{\text{crit}}$  on modeling the H<sub>2</sub> self-shielding.

This paper is structured as follows. Section 2 describes the numerical methods used here, the initial cosmological conditions, and chemical network for the molecular gas. Our results are presented in Section 3. Finally, we discuss and summarize this work in Section 4.

## 2 NUMERICAL METHOD

For simulations of direct collapse within DM haloes, we perform 3D zoom-in cosmological simulations using the Eulerian adaptive mesh refinement (AMR) code Enzo-2.5 (Bryan & Norman 1997; Norman & Bryan 1999; Bryan et al. 2014). To calculate the gravitational dynamics, a particle-mesh  $N$ -body method is implemented (Colella & Woodward 1984; Bryan et al. 1995). The hydrodynamics equations are solved by the piece-wise parabolic solver which is an improved form of the Godunov method (Colella & Woodward 1984). It makes use of the particle mesh technique to solve the DM dynamics and the multi-grid Poisson solver to compute the gravity. For more details of our simulations, we refer the reader to Luo et al. (2016), Luo et al. (2018) and Ardaneh et al. (2018).

### 2.1 Initial conditions

We use fully cosmological initial conditions (ICs) for our models and invoke zoom-in simulations (e.g. Choi et al. 2015; Luo et al. 2016; Shlosman et al. 2016; Luo et al. 2018; Ardaneh et al. 2018).

For the initial conditions, we adopt the MUSIC algorithm (Hahn & Abel 2011), which uses a real-space convolution approach in conjunction with an adaptive multi-grid Poisson solver to generate highly accurate nested density, particle displacement, and velocity fields suitable for multi-scale zoom-in simulations of structure formation in the universe. First, we generate  $1 h^{-1}$  Mpc comoving 128<sup>3</sup> DM-only ICs, initially at  $z = 199$ , and run it without AMR until  $z = 10$ . Using the HOP group finder (Eisenstein & Hut

1998), we select an appropriate DM halo. Then, we generate a zoom-in DM halo with 1024<sup>3</sup> effective resolution in DM and gas, centered on the selected halo position.

The zoom-in region is set to be large enough to cover the initial positions of all selected halo particles. For the DM particles in the zoom-in region, we use 10,223,616 particles which yield an effective DM resolution of about 99 M<sub>⊙</sub>. The baryon resolution is set by the size of the grid cells.

The grid cells are adaptively refined based on the following three criteria: baryon mass, DM mass and Jeans length. A region of the simulation grid is refined by a factor of 2 in length scale, if the gas or DM densities become greater than  $\rho_0 2^{\alpha l}$ , where  $\rho_0$  is the density above which the refinement occurs,  $l$  is the refinement level. We set the ENZO parameter *MinimumMassForRefinementExponent*  $\alpha$  to  $-0.2$ , which reduces the threshold for refinement as higher densities are reached.

We have imposed the condition of at least 16 cells per Jeans length in our simulations, so that no artificial fragmentation would take place (Truelove et al. 1997). In all simulations, we set the maximum refinement level to 15, which is about  $0.23 h^{-1}$  pc comoving.

We use the Planck 2015 for cosmology parameters (Planck Collaboration et al. 2016):  $\Omega_m = 0.3089$ ,  $\Omega_\Lambda = 0.6911$ ,  $\Omega_b = 0.04859$ ,  $\sigma_8 = 0.8159$ ,  $n_s = 0.9667$ , and  $h = 0.6774$ .

### 2.2 Chemical model

We use the publicly available package GRACKLE-3.1.1<sup>1</sup> (Bryan et al. 2014; Smith et al. 2017) to follow thermal and chemical evolution of the collapsing gas. GRACKLE is an open-source chemistry and radiative cooling/heating library suitable for use in numerical astrophysical simulations.

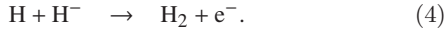
The rate equations of nine chemical species: H, H<sup>+</sup>, He, He<sup>+</sup>, He<sup>++</sup>, e<sup>-</sup>, H<sup>-</sup>, H<sub>2</sub>, and H<sub>2</sub><sup>+</sup> are solved self-consistently along with the hydrodynamics in cosmological simulations. The treatment of H<sub>2</sub> collisional dissociation by H atom collisions is taken from Martin et al. (1996) and accounts for both the temperature and density dependence of this process. The rate coefficients for the three-body reaction to form H<sub>2</sub> is adopted from Forrey (2013), which produces a flat temperature dependence.

We have assumed a dust-free primordial gas and calculated the radiative cooling and heating rates, accounting for collisional excitation, collisional ionization, free-free transitions, recombination, and photoionization heating, depending on the ionizing radiation field. At very high densities, once the H<sub>2</sub> lines become optically-thick, the decrease in the H<sub>2</sub> cooling rate is accounted for (Ripamonti & Abel 2004). The collision-induced emission cooling of H<sub>2</sub> at high densities is also included (Ripamonti & Abel 2004).

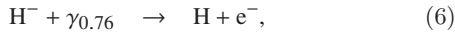
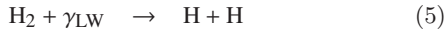
In the direct collapse scenario, a crucial assumption is the suppression of the H<sub>2</sub> formation and cooling. Studies in both semi-analytic analysis and three-dimensional simulations show that a sufficiently strong dissociating Lyman-Werner (LW, 11.2 – 13.6 eV) flux is required to suppress the H<sub>2</sub> cooling entirely. The main pathway for the formation of

<sup>1</sup> <https://grackle.readthedocs.org/>

H<sub>2</sub> in primordial gas is



In the chemical network, H<sub>2</sub> can be reduced either by photo-dissociation of H<sub>2</sub> or photo-detachment of H<sup>-</sup>. Photo-dissociation of the ground state of H<sub>2</sub> happens mostly through absorption in the LW bands to the electronically and vibrationally excited states, and then dissociate to the continuum of the ground state, which is known as the Solomon process (Stecher & Williams 1967). On the other hand, H<sup>-</sup> can be photo-detached by photons with energy above 0.76 eV. The chemical reactions are shown as



where  $\gamma_{\text{LW}}$  and  $\gamma_{0.76}$  represent the photons in the LW bands and the photons with energy above 0.76 eV, respectively. In our work, we perform simulations for a set of H<sub>2</sub> photo-dissociation rate  $k_{\text{H}_2}$  and H<sup>-</sup> photo-detachment rate  $k_{\text{H}^-}$ , and find the critical conditions for suppression of the H<sub>2</sub> formation.

### 2.3 Numerical self-shielding approximations

In regions where the LW bands become optically-thick, the photo-dissociation is much more suppressed, and the cooling rate depends largely on the modeling of the self-shielding. Usually a self-shielding factor  $f_{\text{sh}}$ , which is a function of the H<sub>2</sub> column density,  $N_{\text{H}_2}$ , is adopted to reduce the H<sub>2</sub> cooling rate. However, it remains difficult to make an accurate estimate of the self-shielding factor and the H<sub>2</sub> column densities. In 3D simulations, it is computationally expensive to find the exact self-shielding column density along the different directions. Alternatively, a local method is used, which relies on the estimate of  $N_{\text{H}_2}$  from the local properties of the gas, such as  $N_{\text{H}_2} = n_{\text{H}_2} \lambda$ , where  $n_{\text{H}_2}$  is the H<sub>2</sub> number density, and  $\lambda$  is some characteristic length.

We adopt the improved fitting formula for the self-shielding factor  $f_{\text{sh}}$  from Wolcott-Green et al. (2011) in our simulations, which is defined as

$$f_{\text{sh}} = \frac{0.965}{(1 + x/b_5)^2} + \frac{0.035}{(1 + x)^{0.5}} \exp \left[ -\frac{(1 + x)^{0.5}}{1180} \right], \quad (7)$$

where  $x = N_{\text{H}_2}/5 \times 10^{14} \text{cm}^{-2}$ ,  $b_5 = b/10^5 \text{cm s}^{-1}$  and  $b$  is the Doppler parameter. For the  $N_{\text{H}_2}$  calculation, the improved approximations, e.g., TreeCol algorithm (Clark et al. 2012; Hartwig et al. 2015b,a), six-ray approximation (Yoshida et al. 2007; Glover & Mac Low 2007), or explicit calculation of the column density using HEALPix (Górski et al. 2005; Regan et al. 2016) have been introduced. However, these calculations remain sophisticated and computationally expensive. Instead, we consider three approximations for the characteristic length  $\lambda$ , based on the Jeans length  $\lambda_{\text{Jeans}}$ , Sobolev-like length  $\lambda_{\text{Sob}}$ , and the reduced Jeans length  $\lambda_{\text{Jeans25}} = 0.25 \lambda_{\text{Jeans}}$  proposed by Wolcott-Green et al. (2017). Here  $\lambda_{\text{Sob}} = \rho/|\nabla \rho|$  depends on the gas density  $\rho$  and its spatial gradient.  $\lambda_{\text{Sob}}$  is a method akin to the Sobolev length and is shown in 1D simulations to be accurate in the region where  $n_{\text{H}_2} < 10^4 \text{cm}^{-3}$  (Gnedin et al. 2009; Wolcott-Green et al. 2011).

**Table 1.** Collapse redshift  $z_c$ , dominant cooling  $\Lambda$ , DM virial mass  $M_v$ , central gas temperature  $T_c$  and the halo cosmological spin parameter  $\lambda_{\text{spin}}$  for the simulated haloes, when the maximum refinement level is reached. Here we only list these values for  $k_{\text{H}^-} = 10^{-8} \text{s}^{-1}$ . The dominant cooling  $\Lambda$  refers to models slightly above and below the critical curve shown in Figure 1 as filled (H<sub>1</sub>) and empty (H<sub>2</sub>) symbols, respectively.

	$\lambda$	$\Lambda$	$z_c$	$M_v$	$T_c$	$\lambda_{\text{spin}}$
Halo A	$\lambda_{\text{Jeans}}$	H <sub>2</sub>	17.1	2.5e7	798	0.03
	$\lambda_{\text{Jeans}}$	H <sub>1</sub>	16.8	2.7e7	6217	0.03
	$\lambda_{\text{Jeans25}}$	H <sub>2</sub>	17.3	2.3e7	871	0.03
	$\lambda_{\text{Jeans25}}$	H <sub>1</sub>	16.8	2.7e7	6159	0.03
	$\lambda_{\text{Sob}}$	H <sub>2</sub>	17.3	2.3e7	389	0.03
	$\lambda_{\text{Sob}}$	H <sub>1</sub>	16.8	2.7e7	6142	0.03
Halo B	$\lambda_{\text{Jeans}}$	H <sub>2</sub>	16.7	1.7e7	839	0.01
	$\lambda_{\text{Jeans}}$	H <sub>1</sub>	15.8	2.20e7	6099	0.02
	$\lambda_{\text{Jeans25}}$	H <sub>2</sub>	18.3	1.2e7	901	0.01
	$\lambda_{\text{Jeans25}}$	H <sub>1</sub>	15.7	2.2e7	6123	0.02
	$\lambda_{\text{Sob}}$	H <sub>2</sub>	18.0	1.2e7	482	0.00
	$\lambda_{\text{Sob}}$	H <sub>1</sub>	15.8	2.2e7	6087	0.00
Halo C	$\lambda_{\text{Jeans}}$	H <sub>2</sub>	15.6	2.0e7	874	0.03
	$\lambda_{\text{Jeans}}$	H <sub>1</sub>	16.8	2.7e7	6217	0.03
	$\lambda_{\text{Jeans25}}$	H <sub>2</sub>	15.7	2.0e7	883	0.03
	$\lambda_{\text{Jeans25}}$	H <sub>1</sub>	14.7	2.5e7	6143	0.03
	$\lambda_{\text{Sob}}$	H <sub>2</sub>	15.8	1.9e7	831	0.03
	$\lambda_{\text{Sob}}$	H <sub>1</sub>	14.8	2.4e7	6210	0.03

## 3 RESULTS AND DISCUSSION

### 3.1 The critical curve in the 3D simulations

We have generated the ICs for three chosen haloes. For each halo, we run models applying three different self-shielding approximations, and for each approximation, we have calculated a grid of models in the  $k_{\text{H}_2} - k_{\text{H}^-}$  plane. We checked each model for the dominant gas cooling, atomic or H<sub>2</sub> as they evolved.

To examine the effect of H<sub>2</sub> formation, we monitor the gas dynamics of the simulated haloes and check evolution of their thermodynamic parameters, including temperature and density. Models dominated by atomic or H<sub>2</sub> cooling, have a diverging evolution and can be easily distinguished. Fixing the self-shielding approximations and for each  $k_{\text{H}^-}$ , we found pairs of neighboring models with a dominant atomic and H<sub>2</sub> cooling along the  $k_{\text{H}_2}$  axis. The transition or critical point lies between these pairs of models. For each  $k_{\text{H}^-}$ , we have determined the critical points. Thus, we obtained a sequence of critical points which separate the models with atomic and molecular cooling, and which form a critical curve in the  $k_{\text{H}^-} - k_{\text{H}_2}$  plane.

As we have discussed in the Introduction, a critical curve in the  $k_{\text{H}_2} - k_{\text{H}^-}$  plane can provide a better description for the H<sub>2</sub> suppression (Agarwal et al. 2016; Wolcott-Green et al. 2017). Figure 1 displays our results in the  $k_{\text{H}_2} - k_{\text{H}^-}$  plane, for three different haloes. The empty and filled star symbols represent models dominated by molecular and atomic cooling, respectively, using the self-shielding approximation  $\lambda_{\text{Jeans}}$ .

Note that models of the same halo and with the same value of  $k_{\text{H}^-}$  and the shielding parameter  $\lambda$ , which differ only with  $k_{\text{H}_2}$  will collapse at slightly different redshift. In Table 1,



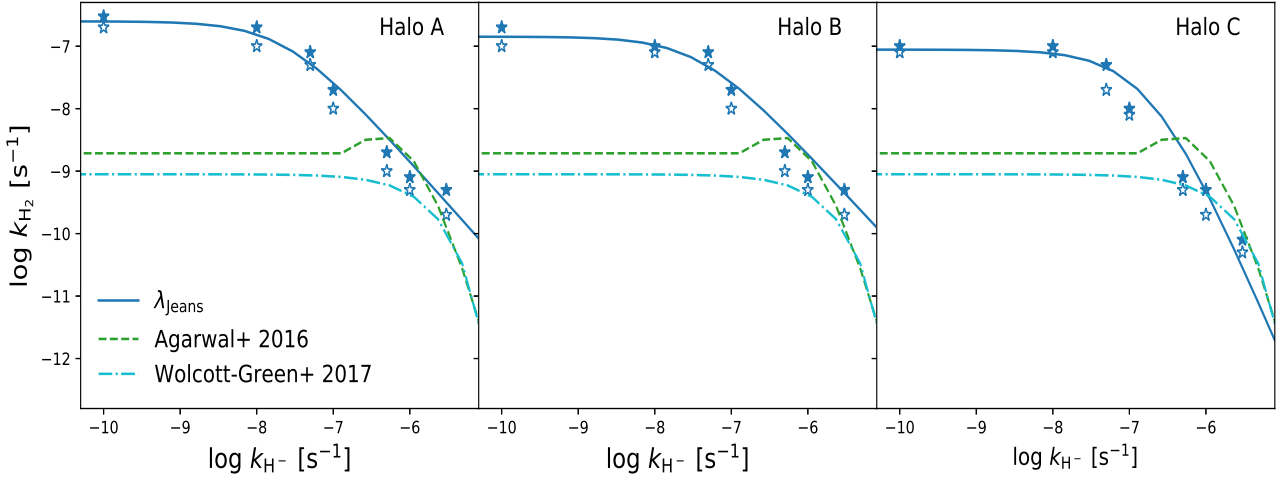


**Figure 1.** Comparison of the 3D critical curve in the  $k_{\text{H}_2} - k_{\text{H}^-}$  plane calculated in this work (blue solid line) with the 1D critical curves in Agarwal et al. (2016) (green dashed line) and Wolcott-Green et al. (2017) (cyan dash-dot line). The green dashed line, as well as our critical blue solid line, are obtained with the same self-shielding approximation  $\lambda_{\text{Jeans}}$ , while the cyan dash-dot line has been obtained with  $\lambda_{\text{Jeans}25}$ . Each line represents the critical boundary in this parameter space above which the H<sub>2</sub> cooling is prevented in our models, for haloes A, B and C. Empty and filled marks show the dominant H<sub>2</sub> and atomic cooling, respectively, measured in our models. The critical dashed line represents the least square fit to critical points determined by us in the 3D runs.

we list the collapse redshifts  $z_c$ , DM virial masses  $M_v$ , the central gas temperatures  $T_c$ , and the halo cosmological spin parameter  $\lambda_{\text{spin}}$ , for the selected models, measured when the maximum refinement level is reached. The gas collapse proceeds from inside out and leads to a central runaway, and this runaway occurs after the gas density exceeds the background DM density (Choi et al. 2013, 2015; Shlosman et al. 2016). The collapse proceeds very rapidly, and the maximum refinement level is reached only in about a few million years (Luo et al. 2016). We stop the simulations when the maximum refinement level has been reached, and measure the required parameters in Table 1. These are listed for different  $\lambda$  approximations and the dominant cooling mechanisms for each approximation. Only models with  $k_{\text{H}^-} = 10^{-8} \text{ s}^{-1}$  are shown in this Table, for simplicity.

In Table 1, models dominated by atomic cooling, i.e., models with  $k_{\text{H}_2}$  above the critical value, collapse with a slight delay compared to a corresponding model with molecular cooling below the critical point. For all models, the collapse redshifts range from 17 to 13, and the virial masses are approximately a few times  $10^7 M_\odot$ . In the H<sub>2</sub> cooling models, the central gas temperature drops down to a few  $\times 100$  K, while in the atomic cooling models, the temperature is kept constant, around 6,000 K.

For a given  $k_{\text{H}^-}$ , the H<sub>2</sub> formation is gradually inhibited with increasing  $k_{\text{H}_2}$ . After determining the critical points for each  $k_{\text{H}^-}$ , we perform the least-square fit and find that the fitting formula can be approximated by

$$k_{\text{H}_2} = a \left( 1 + \frac{k_{\text{H}^-}}{b} \right)^c. \quad (8)$$

The fitting parameters have been listed in Table 2. In Figure 1, for each halo, we display the fitted critical curve in blue solid line with the self-shielding approximation  $\lambda_{\text{Jeans}}$ . Moreover, we have added the critical curve from Agarwal et al. (2016) (green dashed line), which has been calculated with the 1D ENZO code, using the same self-

shielding approximation  $\lambda_{\text{Jeans}}$ , and the same cooling package GRACKLE described in Section 2.2.

Comparison with the critical curve based on the 1D simulations of Agarwal et al. (2016) and our 3D curve calculated under otherwise similar conditions, yields a substantial difference between them, up to two orders of magnitude. Furthermore, we have added additional curve (cyan dash-dot line) from Wolcott-Green et al. (2017) which has been obtained from 1D simulations using the cooling package similar to Shang et al. (2010) and the self-shielding parameter  $\lambda_{\text{Jeans}25}$ . Our results indicate that the critical curve based on our 3D simulations lies much higher than those from the 1D simulations, as seen in Figure 1.

Where exactly the evolution of our models with atomic and molecular cooling bifurcates? Why do models based on the 3D simulations differ profoundly from those in 1D? We discuss the details of this diverging evolution in the following sections.

### 3.2 Impact of the self-shielding column density

Evolution of direct collapse models depends strongly on the dominant cooling mechanism, which affects their temperature profiles and other thermodynamic parameters. Figure 2 exhibits the profiles of the gas temperature, the H<sub>2</sub> fraction  $f_{\text{H}_2}$ , the H<sup>-</sup> fraction  $f_{\text{H}^-}$ , and the ratios of the molecular to the total cooling rates, as functions of the gas density, for the self-shielding parameter  $\lambda_{\text{Jeans}25}$ . Additional approximations,  $\lambda_{\text{Jeans}}$  and  $\lambda_{\text{Sob}}$ , have been evolved as well, but are not shown here. The solid lines show the collapse dominated by the molecular cooling, and the dashed lines correspond to the dominant atomic cooling.

At the initial stage of the collapse, the gas basically goes into the free-fall, and is shock-heated to the halo virial temperature of  $\sim 10^4$  K around the density of  $\sim 10^{-24} \text{ g cm}^{-3}$  at the virial radius. When the gas density reaches about  $10^{-23} \text{ g cm}^{-3}$ , the H<sub>2</sub> formation becomes important for the

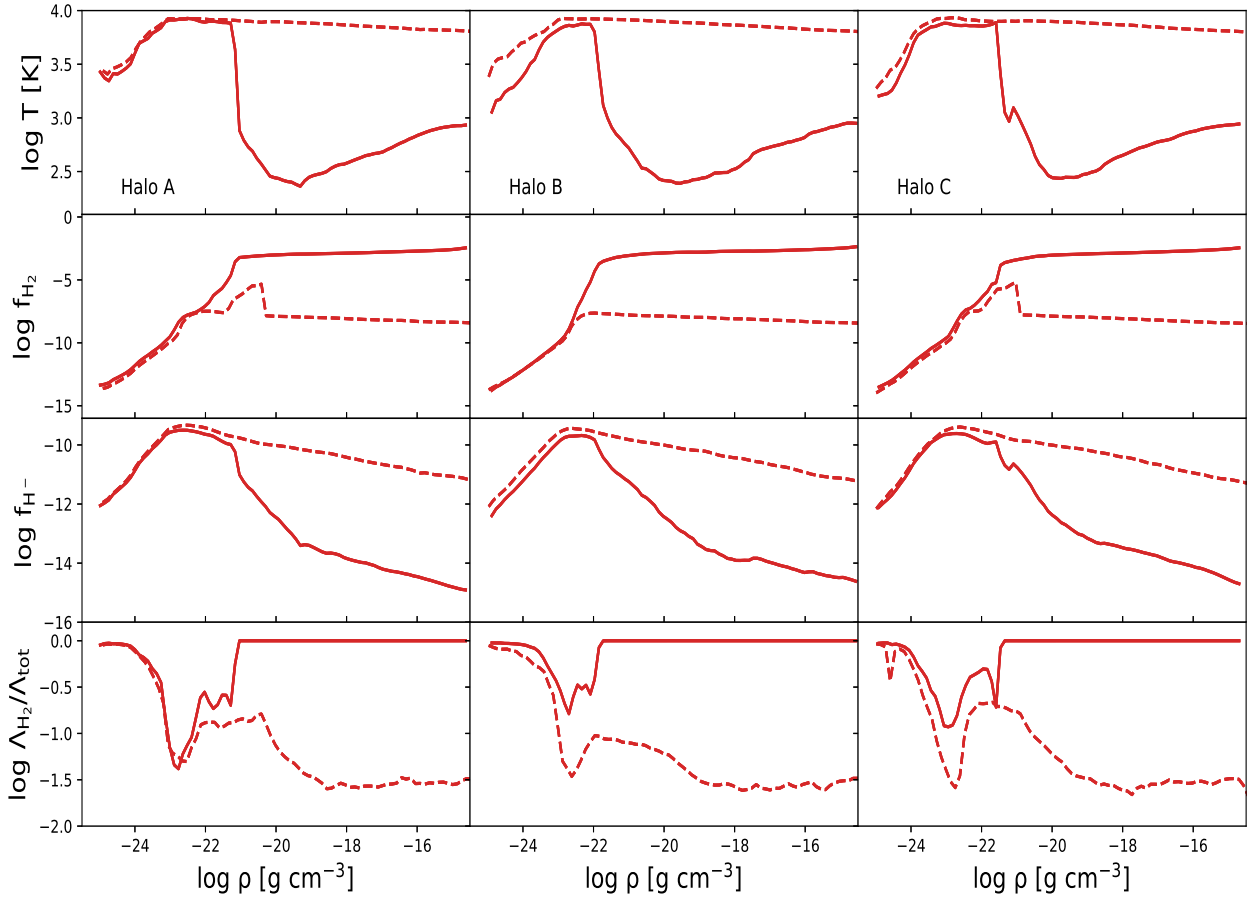


**Figure 2.** Profiles of the gas temperature, of the  $\text{H}_2$  and  $\text{H}^-$  fractions, and the ratios of the molecular to the total cooling rates as a function of the gas density. Only profiles under the condition of  $k_{\text{H}^-} = 10^{-8} \text{ s}^{-1}$  are shown. The curves represent realizations with  $\lambda_{\text{Jeans25}}$  approximation, where the solid lines represent the collapse with the dominant  $\text{H}_2$  cooling and the dashed lines represent the collapse with the atomic cooling.

future evolution of the gas. However, for higher  $k_{\text{H}_2}$ , the photo-dissociation will suppress the  $\text{H}_2$  formation. Hence, the gas still follows the atomic cooling and the collapse proceeds isothermally. The temperature stays nearly constant around 6,000 K, and the  $\text{H}_2$  fraction is kept around its maximum value of  $10^{-8}$  only.

As the gas flows inwards, it remains largely neutral, and the already small  $\text{H}^-$  fraction is slightly decreasing with an increasing density. This is the result of a decreasing fraction of the free electrons required for the  $\text{H}^-$  formation. In cases with the  $\text{H}_2$  cooling being dominant, the total gas cooling rate increases dramatically, causing a substantial drop in the gas temperature, the electron and  $\text{H}^-$  fractions. Around  $10^{-18} \text{ g cm}^{-3}$ , the collisional dissociation of  $\text{H}_2$  begins to suppress the  $\text{H}_2$  cooling. However, the inflow still does not generate the high density/high temperature regime, the so-called ‘zone of no return’ (Inayoshi & Omukai 2012; Fernandez et al. 2014). The compressional heating rate of the collapsing gas decreases substantially due to a lower accretion rate,  $\dot{M}$ , and the sound speed,  $c_s$  — these are related simply by  $\dot{M} \sim c_s^3/G$ . So the heating-cooling balance in the collapsing gas remains at the much lower temperature of the molecular gas.

As we have discussed in the section 2.3, the primordial

gas cooling rate within a DM halo depends on the self-shielding effect of  $\text{H}_2$ . The gas column densities in our models have been calculated using the  $\lambda_{\text{Jeans}}$ ,  $\lambda_{\text{Jeans25}}$  and  $\lambda_{\text{Sob}}$  approximations. In the next step, we test the accuracy of approximating these column densities,  $N_{\text{H}_2}$ . For comparison, we have calculated the actual column density by integrating the  $\text{H}_2$  profile from the outside inwards, and compared it with column densities obtained from  $\lambda_{\text{Jeans}}$ ,  $\lambda_{\text{Jeans25}}$  and  $\lambda_{\text{Sob}}$  approximations.

In Figure 3, we present ratios of the column densities  $N_{\text{H}_2}$  from the adopted self-shielding approximation to that calculated from integrating the  $\text{H}_2$  number density profile. The ratio which stays closer to unity, reflects the more accurate approximation. We display our results for the simulated halo A in the atomic cooling regimes, for fixed  $k_{\text{H}^-} = 10^{-8} \text{ s}^{-1}$ . The results for all three haloes are qualitatively similar, and so haloes B and C have been omitted from this figure. Within the central  $\sim 10 \text{ pc}$ , the  $\lambda_{\text{Jeans}}$  approximation gives a higher estimate of  $N_{\text{H}_2}$  by a factor of 4, while usage of  $\lambda_{\text{Sob}}$  leads to the estimate which is too low. The  $\lambda_{\text{Sob}}$  method also shows a relatively large scatter along the radius. However, the ratio obtained from  $\lambda_{\text{Jeans25}}$  to that determined from simulations lies much closer to unity, and provide a more accurate estimate of the  $\text{H}_2$  self-shielding.

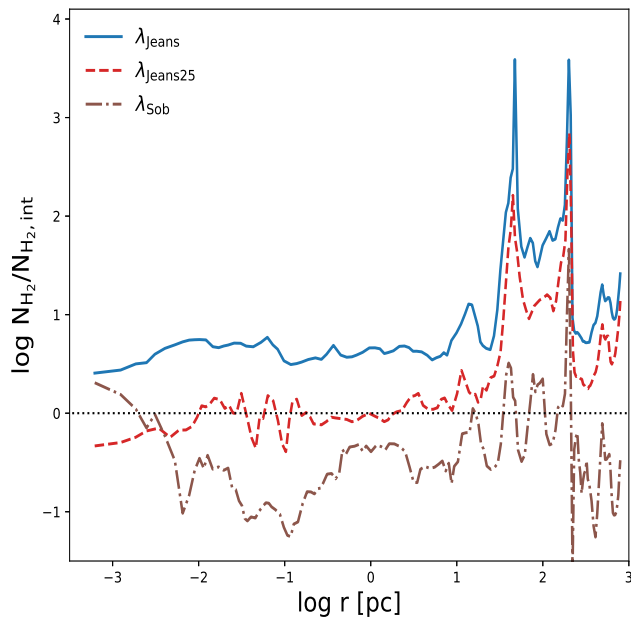


**Figure 3.** Comparison between the column density approximations. The ratios of the H<sub>2</sub> column density  $N_{\text{H}_2}$  to the actual column density  $N_{\text{H}_2,\text{int}}$  are displayed. Approximations for  $\lambda_{\text{Jeans}}$ ,  $\lambda_{\text{Jeans25}}$  and  $\lambda_{\text{Sob}}$ , are shown as the blue solid, red dashed, and brown dash-dot lines, respectively. The black dotted line is drawn to delineate the ratio of unity.

**Table 2.** Least-square fitting parameters for the critical curves determined from 3D numerical simulations presented in this work (see eq.7).

	$\lambda$	a	b	c
Halo A	$\lambda_{\text{Jeans}}$	2.5e-07	2.4e-08	-1.4
	$\lambda_{\text{Jeans25}}$	3.1e-08	1.2e-08	-1.6
	$\lambda_{\text{Sob}}$	1.1e-10	1.2e-07	-1.9
Halo B	$\lambda_{\text{Jeans}}$	1.4e-07	3.9e-08	-1.3
	$\lambda_{\text{Jeans25}}$	3.2e-08	1.3e-07	-1.6
	$\lambda_{\text{Sob}}$	1.1e-10	1.1e-07	-2.0
Halo C	$\lambda_{\text{Jeans}}$	8.8e-08	1.9e-07	-2.9
	$\lambda_{\text{Jeans25}}$	3.2e-08	3.1e-07	-3.1
	$\lambda_{\text{Sob}}$	1.2e-10	1.0e-07	-2.0

The self-shielding factors  $f_{\text{sh}}$  are plotted in Figure 4 for the three approximations,  $\lambda_{\text{Jeans}}$ ,  $\lambda_{\text{Jeans25}}$  and  $\lambda_{\text{Sob}}$ , from left to right, respectively. The solid lines represent the  $f_{\text{sh}}$  in the H<sub>2</sub> cooling cases, and the dashed lines in the atomic cooling cases. Outside the central  $\sim 10$  pc region of the collapse,  $f_{\text{sh}}$  is insensitive to the choice of  $\lambda$ . But within the central 10 pc, the H<sub>2</sub> fraction is sharply increasing (see the second row of Figure 2), and the  $\lambda$  approximation becomes important for the  $f_{\text{sh}}$  calculation.

Finally, we compared the critical curves calculated in the  $k_{\text{H}^-} - k_{\text{H}_2}$  plane with three different prescriptions for the self-shielding (Figure 5). This has been performed for each of the three DM haloes. The fitted curves are given in blue solid, red dashed and brown dash-dot lines for  $\lambda_{\text{Jeans}}$  (see also

Figure 1),  $\lambda_{\text{Jeans25}}$  and  $\lambda_{\text{Sob}}$ , respectively. The least-square fitting parameters have been listed in Table 2.

The critical curve for  $\lambda_{\text{Jeans}}$  shows that it lies consistently above that the critical curve for  $\lambda_{\text{Sob}}$ . So the required radiation intensity to suppress the H<sub>2</sub> formation, therefore, should be stronger as well. The critical curve is sensitive, by about one order of magnitude, to the choice of the column density approximation used, especially for  $k_{\text{H}^-} < 10^{-7} \text{ s}^{-1}$ . For  $k_{\text{H}_2} > 10^{-7} \text{ s}^{-1}$ , the curve drops down sharply, because the H<sup>+</sup> becomes fully photo-detached and H<sub>2</sub> cannot form via H<sup>+</sup>. We do not adopt the fitting formula given by the 1D simulations of Wolcott-Green et al. (2017) and Agarwal et al. (2016), which fit the critical curve with an exponential tail at higher  $k_{\text{H}^-}$ . In fact we find that the decay is better fit by a power-law shape, with an index of about  $-1.6$ . The reason for this is because in the 3D simulations, the spatial variations in density will enhance the H<sub>2</sub> formation from H<sup>+</sup>. This is a crucial difference between the 1D and 3D simulations.

### 3.3 Calculation of $J_{\text{crit}}$ from the critical curve

In Figure 5, the two diagonal dotted lines illustrate the relationship between  $k_{\text{H}_2}$  and  $k_{\text{H}^-}$  with varying intensity for a T4 (lower) and T5 (upper) spectral shapes, respectively. We are able to reproduce the critical intensity  $J_{\text{crit}}$  obtained in previous studies by assuming their fixed blackbody spectral shapes. The critical values lie at the intersection of the diagonal dotted lines crossing the critical curves.

In Table 3, we list the critical intensity  $J_{\text{crit}}$  for a blackbody spectra of T5 and T4, adopted from previous studies. The second column of Table 3 displays the self-shielding  $\lambda$  approximation adopted in these studies. The third and fourth columns show  $J_{\text{crit}}$  by assuming a T5 (lower) and T4 (upper) spectral shapes, respectively. The last two columns show the numerical methods used, as well as the methods applied for the self-shielding factor estimates. We have successfully reproduced the calculations of  $J_{\text{crit}}$ . Those lie at the intersections of the diagonal dotted lines with the critical curves shown in Figures 1 and 5. The values of  $J_{\text{crit}}$  reproduced from the previous 1D simulations by Wolcott-Green et al. (2017) and Agarwal et al. (2016) are also shown in the Table as a comparison.

We have obtained  $J_{\text{crit}}$  from our three simulated haloes. The value of  $J_{\text{crit}}$  varies from halo to halo, but the variations are within a factor of two. This is shown as a range of values in Table 3. By comparing  $J_{\text{crit}}$  calculated in 3D simulations applying the  $\lambda_{\text{Jeans}}$  approximation, our  $J_{\text{crit}}$  with T5 is consistent with that from Shang et al. (2010). It is about 30% higher in comparison with Hartwig et al. (2015a). Our  $J_{\text{crit}}$  with T4 is consistent with that from Shang et al. (2010), but is smaller by one order of magnitude with that from Latif et al. (2014a). Note, that Latif et al. (2014a) used a different chemical network for H<sub>2</sub> formation, KROME<sup>2</sup> (Grassi et al. 2014). Therefore, the chemical reactions and rate coefficients could cause the difference in  $J_{\text{crit}}$  values, as pointed out by Glover (2015a) and Glover (2015b).

Using different  $\lambda$  approximation, the values of  $J_{\text{crit}}$  differ by up to two orders of magnitude. In our calculations, the  $J_{\text{crit}}$  in  $\lambda_{\text{Sob}}$  approximation is smaller than that in  $\lambda_{\text{Jeans}}$  by

<sup>2</sup> <https://www.kromepackage.org/>

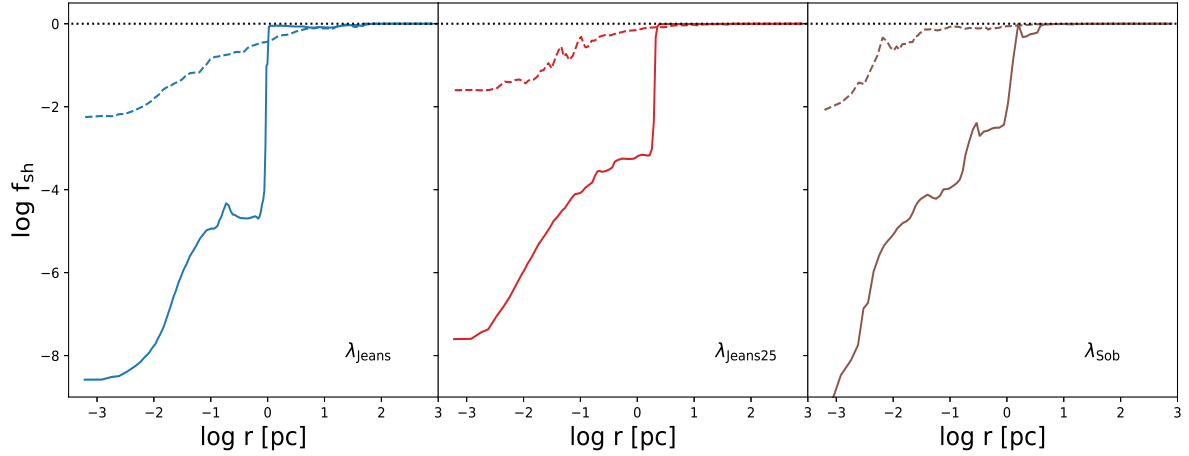


**Figure 4.** Profiles of the self-shielding factor as functions of radius. The solid lines represent the collapse with the dominant  $\text{H}_2$  cooling and the dashed lines represent the collapse with the dominant atomic cooling. From the left to the right panels, approximations for  $\lambda_{\text{Jeans}}$ ,  $\lambda_{\text{Jeans25}}$  and  $\lambda_{\text{Sob}}$ , are shown as blue, red, and brown lines, respectively. The black dotted line is drawn to delineate the ratio of unity.

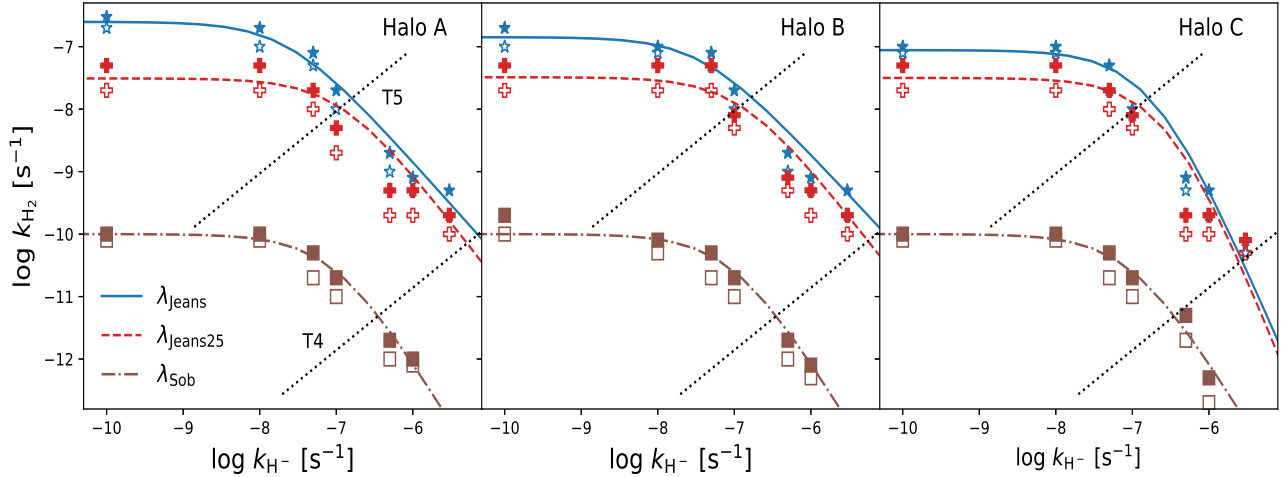


**Figure 5.** The critical curves in the  $k_{\text{H}_2} - k_{\text{H}^-}$  plane (see caption for Figure 1), using three different methods to calculate the self-shielding characteristic length  $\lambda$ ; namely,  $\lambda_{\text{Jeans}}$  (blue solid line, shown also in Fig. 1),  $\lambda_{\text{Jeans25}}$  (red dashed line), and  $\lambda_{\text{Sob}}$  (brown dash-dot line). The two diagonal black dotted lines represent the rates with varying intensity for the T4 (lower) and T5 spectrum (upper), respectively.

**Table 3.** Compilations of  $J_{\text{crit}}$  values in units of  $J_{\text{LW},21}$  in earlier works using the T5 or T4 black-body spectra. The critical values are obtained at the intersection of the diagonal dotted lines with the critical curves shown in Figures 1 and 5. The last column lists the method used for the self-shielding approximation.

Authors	$\lambda$	$J_{\text{crit}, \text{T}_5}$	$J_{\text{crit}, \text{T}_4}$	Methods	Approximations
This Work	$\lambda_{\text{Jeans}}$	1e4-2e4	13-42	3D	Wolcott-Green et al. (2011)
	$\lambda_{\text{Jeans25}}$	7e3-8e3	13-27	3D	Wolcott-Green et al. (2011)
	$\lambda_{\text{Sob}}$	75-82	1.6-1.9	3D	Wolcott-Green et al. (2011)
Shang et al. (2010)	$\lambda_{\text{Jeans}}$	1.2e4	39	1D	Draine & Bertoldi (1996)
Shang et al. (2010)	$\lambda_{\text{Jeans}}$	1e4-1e5	30-300	3D	Draine & Bertoldi (1996)
Latif et al. (2014a)	---	---	400-1500	3D	Wolcott-Green et al. (2011)
Latif et al. (2014a)	---	---	30-40	1D	Wolcott-Green et al. (2011)
Sugimura et al. (2014)	$\lambda_{\text{Jeans}}$	1.4e3	59.8	1D	Wolcott-Green et al. (2011)
Hartwig et al. (2015a)	$\lambda_{\text{Jeans}}$	3.5e3-5.5e3	---	3D	Wolcott-Green et al. (2011)
Agarwal et al. (2016)	$\lambda_{\text{Jeans}}$	1.5e3	19.4	1D	Wolcott-Green et al. (2011)
Wolcott-Green et al. (2017)	$\lambda_{\text{Jeans25}}$	6.6e2	19.3	1D	Wolcott-Green et al. (2011)



almost two orders of magnitude. In addition, for a softer spectrum, e.g., T4, the values of  $J_{\text{crit}}$  are smaller than the values derived from a harder spectrum with T5, again by up to two orders of magnitude. For the softer spectrum, the radiation field above 0.76 eV lead to an increase in  $k_{\text{H}^-}$ . With increasing  $k_{\text{H}^-}$ , the required  $k_{\text{H}_2}$  or  $J_{\text{crit}}$  to suppress the  $\text{H}_2$  cooling decreases.

Intensities estimated from our 3D simulations tend to be larger compared to those obtained in 1D simulations. For example, the values of  $J_{\text{crit},\text{T5}}$  from 1D simulations by Sugimura et al. (2014) and Agarwal et al. (2016) are one order of magnitude smaller than those calculated from 3D simulations by Shang et al. (2010) and by our work. The difference in  $J_{\text{crit}}$  between the 1D and 3D simulations has been also found by Hartwig et al. (2015a) and Latif et al. (2014a), who used the single-temperature blackbody spectral shape. The difference between the 1D and 3D simulations can be triggered by the spatial variations in the temperature and density within the accretion flow (e.g., Shang et al. 2010).

Previous studies which obtained  $J_{\text{crit}}$ , used the single-temperature blackbody spectra. Consequently, these studies obtained only a single point each on the  $k_{\text{H}_2} - k_{\text{H}^-}$  plane. By comparing  $J_{\text{crit}}$  obtained from previous studies with our values from the critical curve, we find the critical curve provides a more general and compelling way to determine the critical intensity. The single blackbody results from previous works have been reproduced using this curve.

#### 4 DISCUSSION AND CONCLUDING REMARKS

We have calculated the conditions for suppressing the formation of  $\text{H}_2$  in the direct collapse scenario towards the SMBH seeds, within DM haloes. Using series of 3D numerical simulations we have obtained the critical intensity of the background UV radiation by constructing the critical curves in the  $k_{\text{H}_2} - k_{\text{H}^-}$  parameter plane, separating models with dominant atomic and molecular cooling. We have also shown the dependence of the critical conditions on the choice of the  $\text{H}_2$  column density approximation in the self-shielding calculation. Our main findings can be summarized as follows.

- We have verified that there exists a critical curve in the  $k_{\text{H}_2} - k_{\text{H}^-}$  parameter plane, above which the  $\text{H}_2$  cooling is suppressed, and the atomic cooling dominates.
- We have provided a fitting formula for this critical curve and found that the fitted curve based on the 3D numerical simulations differs substantially from that obtained in the 1D simulations, both in its position in the  $k_{\text{H}_2} - k_{\text{H}^-}$  parameter plane and in its shape.
- We have compared the critical curves calculated in 3D simulations using three different  $\text{H}_2$  column density approximations in the self-shielding calculation,  $\lambda_{\text{Jeans}}$ ,  $\lambda_{\text{Jeans25}}$  and  $\lambda_{\text{Sob}}$ . These approximations correspond to the Jeans length, a fraction of the Jeans length and the Sobolev length, respectively. We find that the characteristic length-scale for shielding can be improved by using  $\lambda_{\text{Jeans25}}$ , which is four times smaller than the local Jeans length.

The direct collapse models involve the gas accretion within the DM haloes, resulting in the SMBH seeds of  $\sim 10^4 - 10^6 M_\odot$ . It circumvents the difficulties associated with

the growth of the Pop III black hole remnants from stellar masses to the SMBH masses found in the galactic centers.

To sustain a high inflow rate of  $\sim 0.1 - 1 M_\odot \text{ yr}^{-1}$ , the  $\text{H}_2$  formation should be inhibited in the primordial gas. To prevent accretion flow fragmentation induced by the  $\text{H}_2$  cooling, the halo must be exposed to the background UV radiation whose intensity exceeds  $J_{\text{crit}}$ . To obtain the  $J_{\text{crit}}$ , a single blackbody or power-law spectra have been assumed in the literature to model the background radiation. However in realistic situations, this radiation field is time-dependent, and a simple spectral shape model cannot capture all the intricacies associated with the flux variability, anisotropy and changing spectral shape. Therefore, it is advantageous to use an alternative approach and deal with the critical intensity that is defined in a more general way, by a combination of  $k_{\text{H}_2}$  and  $k_{\text{H}^-}$ . There is no need to make any initial assumptions on the properties of the underlying radiation.

We have tested this approach in the fully 3D simulations, and found that a critical curve can exist in the  $k_{\text{H}_2} - k_{\text{H}^-}$  parameter plane. The critical curve position and shape is strongly affected by replacing the 1D with more realistic simulations in the 3D. Moreover, we have successfully applied a new fitting formula to the critical curve in this parameter space, and compared this curve to those obtained in the 1D simulations. The main outcome of this comparison is that the critical curve in the 3D simulations lies substantially higher than that from the 1D simulations, by about two orders of magnitude.

Our analysis also includes the  $\text{H}_2$  column density approximations for the self-shielding factor calculation. As the gas flows inwards, its density increases, and so is the  $\text{H}_2$  number density. When the  $\text{H}_2$  column densities increase (e.g.,  $N_{\text{H}_2} > 10^{14} \text{ cm}^{-2}$ ), the photo-dissociation is suppressed because the region becomes optically-thick for the Lyman-Werner photons. The treatment of the gas cooling, therefore, depends on the  $\text{H}_2$  self-shielding approximation. The three cases considered here,  $\lambda_{\text{Jeans}}$ ,  $\lambda_{\text{Jeans25}}$ , and  $\lambda_{\text{Sob}}$ , which approximate the characteristic length, provide the column densities, some of which differ from the actual column densities estimated directly from the simulations. The  $\lambda_{\text{Jeans}}$  approximation overestimates the shielding, while the  $\lambda_{\text{Sob}}$  approximation significantly underestimates it. We find that  $\lambda_{\text{Jeans25}}$  yields the most accurate approach to the true characteristic self-shielding.

In summary, the 3D simulations in tandem with the  $\lambda_{\text{Jeans25}}$  approximation for the column density, provide a substantial improvement over the 1D simulation with fixed spectral shapes of the background UV radiation.

#### ACKNOWLEDGEMENTS

We thank the Enzo and YT support team for help. All the analysis has been conducted using yt (Turk et al. 2011), <http://yt-project.org/>. This work has been partially supported by the Hubble Theory grant HST-AR-14584 (to I.S.), and by JSPS KAKENHI grant 16H02163 (to I.S.) and 17H01111 (to K.N.). I.S. and K.N. are grateful for a generous support from the International Joint Research Promotion Program at Osaka University. The STScI is operated by the AURA, Inc., under NASA contract NAS5-26555. T.F. acknowledge support from the National Key R&D Pro-

gram of China No. 2017YFA0402600, and NSFC grants No. 11525312, 11890692. Numerical simulations have been performed on Tianhe-2 at the National Supercomputer Center in Guangzhou, on Supercomputer at the Shanghai Astronomical Observatory, as well as on the LCC Linux Cluster of the University of Kentucky.

## REFERENCES

- Abel T., Anninos P., Zhang Y., Norman M. L., 1997, *New Astron.*, **2**, 181
- Agarwal B., Khochfar S., Johnson J. L., Neistein E., Dalla Vecchia C., Livio M., 2012, *MNRAS*, **425**, 2854
- Agarwal B., Smith B., Glover S., Natarajan P., Khochfar S., 2016, *MNRAS*, **459**, 4209
- Ahn K., Shapiro P. R., Iliev I. T., Mellema G., Pen U.-L., 2009, *ApJ*, **695**, 1430
- Ardaneh K., Luo Y., Shlosman I., Nagamine K., Wise J. H., Begelman M. C., 2018, *MNRAS*, **479**, 2277
- Bañados E., et al., 2018, *Nature*, **553**, 473
- Begelman M. C., 2010, *MNRAS*, **402**, 673
- Begelman M. C., Rees M. J., 1978, *MNRAS*, **185**, 847
- Begelman M. C., Shlosman I., 2009, *ApJ*, **702**, L5
- Begelman M. C., Volonteri M., Rees M. J., 2006, *MNRAS*, **370**, 289
- Begelman M. C., Rossi E. M., Armitage P. J., 2008, *MNRAS*, **387**, 1649
- Bromm V., Loeb A., 2003, *ApJ*, **596**, 34
- Bryan G. L., Norman M. L., 1997, in Clarke D. A., West M. J., eds, *Astronomical Society of the Pacific Conference Series Vol. 12, Computational Astrophysics; 12th Kingston Meeting on Theoretical Astrophysics*. p. 363 ([arXiv:astro-ph/9710186](https://arxiv.org/abs/astro-ph/9710186))
- Bryan G. L., Norman M. L., Stone J. M., Cen R., Ostriker J. P., 1995, *Computer Physics Communications*, **89**, 149
- Bryan G. L., et al., 2014, *The Astrophysical Journal Supplement Series*, **211**, 19
- Choi J.-H., Shlosman I., Begelman M. C., 2013, *ApJ*, **774**, 149
- Choi J.-H., Shlosman I., Begelman M. C., 2015, *MNRAS*, **450**, 4411
- Chon S., Latif M. A., 2017, *MNRAS*, **467**, 4293
- Chon S., Hirano S., Hosokawa T., Yoshida N., 2016, *ApJ*, **832**, 134
- Ciardi B., Ferrara A., 2005, *Space Sci. Rev.*, **116**, 625
- Ciardi B., Ferrara A., Abel T., 2000, *ApJ*, **533**, 594
- Clark P. C., Glover S. C. O., Klessen R. S., 2012, *MNRAS*, **420**, 745
- Colella P., Woodward P. R., 1984, *Journal of Computational Physics*, **54**, 174
- Dijkstra M., Haiman Z., Mesinger A., Wyithe J. S. B., 2008, *MNRAS*, **391**, 1961
- Dijkstra M., Ferrara A., Mesinger A., 2014, *MNRAS*, **442**, 2036
- Draine B. T., Bertoldi F., 1996, *ApJ*, **468**, 269
- Dunn G., Bellovary J., Holley-Bockelmann K., Christensen C., Quinn T., 2018, *ApJ*, **861**, 39
- Eisenstein D. J., Hut P., 1998, *ApJ*, **498**, 137
- Fan X., et al., 2003, *AJ*, **125**, 1649
- Fernandez R., Bryan G. L., Haiman Z., Li M., 2014, *MNRAS*, **439**, 3798
- Forrey R. C., 2013, *ApJ*, **773**, L25
- Ge Q., Wise J. H., 2017, *MNRAS*, **472**, 2773
- Glover S. C. O., 2015a, *MNRAS*, **451**, 2082
- Glover S. C. O., 2015b, *MNRAS*, **453**, 2901
- Glover S. C. O., 2016, *arXiv e-prints*, p. [arXiv:1610.05679](https://arxiv.org/abs/1610.05679)
- Glover S. C. O., Jappsen A. K., 2007, *ApJ*, **666**, 1
- Glover S. C. O., Mac Low M.-M., 2007, *ApJS*, **169**, 239
- Gnedin N. Y., Tassis K., Kravtsov A. V., 2009, *ApJ*, **697**, 55
- Górski K. M., Hivon E., Banday A. J., Wandelt B. D., Hansen F. K., Reinecke M., Bartelmann M., 2005, *ApJ*, **622**, 759
- Grassi T., Bovino S., Schleicher D. R. G., Prieto J., Seifried D., Simoncini E., Gianturco F. A., 2014, *MNRAS*, **439**, 2386
- Greif T. H., Johnson J. L., Bromm V., Klessen R. S., 2007, *ApJ*, **670**, 1
- Greif T. H., Springel V., White S. D. M., Glover S. C. O., Clark P. C., Smith R. J., Klessen R. S., Bromm V., 2011, *ApJ*, **737**, 75
- Haardt F., Madau P., 2012, *ApJ*, **746**, 125
- Habouzit M., Volonteri M., Latif M., Dubois Y., Peirani S., 2016, *MNRAS*, **463**, 529
- Haehnelt M. G., Rees M. J., 1993, *MNRAS*, **263**, 168
- Hahn O., Abel T., 2011, *MNRAS*, **415**, 2101
- Haiman Z., Abel T., Rees M. J., 2000, *ApJ*, **534**, 11
- Hartwig T., Glover S. C. O., Klessen R. S., Latif M. A., Volonteri M., 2015a, *MNRAS*, **452**, 1233
- Hartwig T., Clark P. C., Glover S. C. O., Klessen R. S., Sasaki M., 2015b, *ApJ*, **799**, 114
- Holzbaumer L. N., Furlanetto S. R., 2012, *MNRAS*, **419**, 718
- Inayoshi K., Haiman Z., 2014, *MNRAS*, **445**, 1549
- Inayoshi K., Omukai K., 2012, *MNRAS*, **422**, 2539
- Inayoshi K., Tanaka T. L., 2015, *MNRAS*, **450**, 4350
- Johnson J. L., Dijkstra M., 2017, *A&A*, **601**, A138
- Johnson J. L., Khochfar S., Greif T. H., Durier F., 2011, *MNRAS*, **410**, 919
- Koushiappas S. M., Bullock J. S., Dekel A., 2004, *MNRAS*, **354**, 292
- Latif M. A., Schleicher D. R. G., Schmidt W., Niemeyer J., 2013, *MNRAS*, **433**, 1607
- Latif M. A., Bovino S., Van Borm C., Grassi T., Schleicher D. R. G., Spaans M., 2014a, *MNRAS*, **443**, 1979
- Latif M. A., Schleicher D. R. G., Bovino S., Grassi T., Spaans M., 2014b, *ApJ*, **792**, 78
- Latif M. A., Bovino S., Grassi T., Schleicher D. R. G., Spaans M., 2015, *MNRAS*, **446**, 3163
- Latif M. A., Omukai K., Habouzit M., Schleicher D. R. G., Volonteri M., 2016, *ApJ*, **823**, 40
- Loeb A., Rasio F. A., 1994, *ApJ*, **432**, 52
- Luo Y., Nagamine K., Shlosman I., 2016, *MNRAS*, **459**, 3217
- Luo Y., Ardaneh K., Shlosman I., Nagamine K., Wise J. H., Begelman M. C., 2018, *MNRAS*, **476**, 3523
- Lupi A., Colpi M., Devecchi B., Galanti G., Volonteri M., 2014, *MNRAS*, **442**, 3616
- Martin P. G., Schwarz D. H., Mandy M. E., 1996, *ApJ*, **461**, 265
- Mayer L., Kazantzidis S., Escala A., Callegari S., 2010, *Nature*, **466**, 1082
- Milosavljević M., Bromm V., Couch S. M., Oh S. P., 2009, *ApJ*, **698**, 766
- Miyake S., Stancil P. C., Sadeghpour H. R., Dalgarno A., McLaughlin B. M., Forrey R. C., 2010, *ApJ*, **709**, L168
- Mortlock D. J., et al., 2011, *Nature*, **474**, 616
- Norman M. L., Bryan G. L., 1999, in Miyama S. M., Tomisaka K., Hanawa T., eds, *Astrophysics and Space Science Library Vol. 240, Numerical Astrophysics*. p. 19 ([arXiv:astro-ph/9807121](https://arxiv.org/abs/astro-ph/9807121)), doi:10.1007/978-94-011-4780-4\_3
- Omukai K., 2001, *ApJ*, **546**, 635
- Planck Collaboration et al., 2016, *A&A*, **594**, A13
- Rees M. J., 1984, *ARA&A*, **22**, 471
- Regan J. A., Downes T. P., 2018, *MNRAS*, **475**, 4636
- Regan J. A., Haehnelt M. G., 2009, *MNRAS*, **396**, 343
- Regan J. A., Johansson P. H., Wise J. H., 2016, *MNRAS*, **459**, 3377
- Ripamonti E., Abel T., 2004, *MNRAS*, **348**, 1019
- Schleicher D. R. G., Spaans M., Glover S. C. O., 2010, *ApJ*, **712**, L69
- Shang K., Bryan G. L., Haiman Z., 2010, *MNRAS*, **402**, 1249
- Shapiro S. L., Teukolsky S. A., 1985, *ApJ*, **298**, 58

- Shlosman I., Choi J.-H., Begelman M. C., Nagamine K., 2016, [MNRAS](#), **456**, 500
- Smith B. D., et al., 2017, [MNRAS](#), **466**, 2217
- Stecher T. P., Williams D. A., 1967, [ApJ](#), **149**, L29
- Sugimura K., Omukai K., Inoue A. K., 2014, [MNRAS](#), **445**, 544
- Truelove J. K., Klein R. I., McKee C. F., Holliman John H. I., Howell L. H., Greenough J. A., 1997, [ApJ](#), **489**, L179
- Turk M. J., Smith B. D., Oishi J. S., Skory S., Skillman S. W., Abel T., Norman M. L., 2011, [The Astrophysical Journal Supplement Series](#), **192**, 9
- Venemans B. P., et al., 2017, [ApJ](#), **851**, L8
- Volonteri M., Rees M. J., 2006, [ApJ](#), **650**, 669
- Willott C. J., et al., 2010, [AJ](#), **139**, 906
- Wise J. H., Abel T., 2008, [ApJ](#), **685**, 40
- Wolcott-Green J., Haiman Z., Bryan G. L., 2011, [MNRAS](#), **418**, 838
- Wolcott-Green J., Haiman Z., Bryan G. L., 2017, [MNRAS](#), **469**, 3329
- Wu X.-B., et al., 2015, [Nature](#), **518**, 512
- Yoshida N., Oh S. P., Kitayama T., Hernquist L., 2007, [ApJ](#), **663**, 687
- Yue B., Ferrara A., Salvaterra R., Xu Y., Chen X., 2013, [MNRAS](#), **433**, 1556
- Yue B., Ferrara A., Salvaterra R., Xu Y., Chen X., 2014, [MNRAS](#), **440**, 1263
- Yue B., Ferrara A., Pacucci F., Omukai K., 2017, [ApJ](#), **838**, 111
- Zel'dovich Y. B., Podurets M. A., 1965, [Azh](#), **42**, 963

This paper has been typeset from a  $\text{\TeX}/\text{\LaTeX}$  file prepared by the author.